ACS central science

http://pubs.acs.org/journal/acscii

Research Article

Improved Ion Transport in Hydrogel-Based Nanofluidics for Osmotic Energy Conversion

Weipeng Chen, Qianru Zhang, Yongchao Qian, Weiwen Xin, Dezhao Hao, Xiaolu Zhao, Congcong Zhu, Xiang-Yu Kong, Benzhuo Lu, Lei Jiang, and Liping Wen*

Cite This: ACS Cent. Sci. 2020, 6, 2097−2104

Read Online

ACCESS | Metrics & More | Article Recommendations | Supporting Information

ABSTRACT: In nature, ultrafast signal transfer based on ion transport, which is the foundation of biological processes, commonly works in a hydrogel−water mixed mechanism. Inspired by organisms' hydrogel-based system, we introduce hydrogel into nanofluidics to prepare a hydrogel hybrid membrane. The introduction of a space charged hydrogel improves the ion selectivity evidently. Also, a power generator based on the hydrogel hybrid membrane shows an excellent energy conversion property; a maximum power density up to 11.72 W/m^2 is achieved at a 500-fold salinity gradient. Furthermore, the membrane shows excellent mechanical properties. These values are achievable, which indicates our membrane's huge potential applications in osmotic energy conversion.

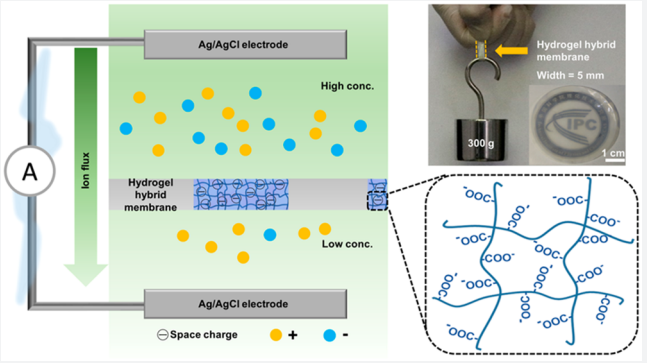

INTRODUCTION

Ion transport in a charged channel with dimensions comparable to the Debye length shows different behavior from the bulk.[1,2] The charge-governed ion transport, for example, ion selectivity, has drawn enormous research attention.[3−7] On the basis of this unique phenomenon, a number of applications have been explored such as sensing devices,[8] water desalination,[9] and ionic neural electrodes.[10] Also, in recent years, the ion selective membrane has been used to harvest osmotic energy from the salinity gradient between seawater and river water, which is a promising alternative to fossil fuel burning owing to its cleanliness, renewability, and abundance.[11−16] Nevertheless, state-of-the-art ion selective membranes are caught in low ion selectivity or high internal resistance, leading to the poor performance.[17,18] Therefore, investigating the efficient transmembrane transport of ions and, meanwhile, exploiting membranes with high selectivity and conductance are desperately demanded.

Hydrogel, a "soft and wet" material with a three-dimensional (3D) network structure, shows potential in facilitating fast mass transport of ions/electrons with its interconnected pathways and the ability of being space charged.[19,20] However, the pore size of hydrogel is generally on the micrometer scale, which would lead to the poor performance. In nature, various hydrogels with different forms arose in organisms to satisfy the requirements of different functions based on charge-governed ion transport.[21−23] For example, in order to defend itself and incapacitate prey, the electric eel can generate discharges up to 600 V from gradients of ions, contributed by the unique hydrogel electric organs with excellent ion selectivity and low internal resistance.[22] In human bodies, skeletal muscles, which help the signal transmission, are composed of well-ordered hydrogel fibers with a size range from micrometers to nanometers.[23] Therefore, exploring the effect of structural variations of hydrogels on ion transport would lay the groundwork for a deeper understanding of efficient ion transport. Also, incorporating hydrogel into nanofluidics may enable new properties to solve the bottleneck of state-of-the-art systems.

Herein, inspired by the natural systems, we designed a hydrogel hybrid membrane by constructing hydrogel nanofibers in 1D channels of a polycarbonate (PC) membrane through radical initiated polymerization. The supporting framework is a commercialized polycarbonate (PC) film with cylindrical channels, and acrylic acid (AAc)−*co*-acrylamide (AAm)−*co*-methyl methacrylate (MMA) hydrogels are filled in the channels (Figure 1). Compared with the present nanofluidics, our membrane works in an organism-like hydrogel−water ambient. The hybrid membrane which features unique nanochannels and space negative charges exhibits high cation selectivity (Figure 1a). Under a salinity

Received: August 5, 2020
Published: October 13, 2020

https://dx.doi.org/10.1021/acscentsci.0c01054
ACS Cent. Sci. 2020, 6, 2097−2104

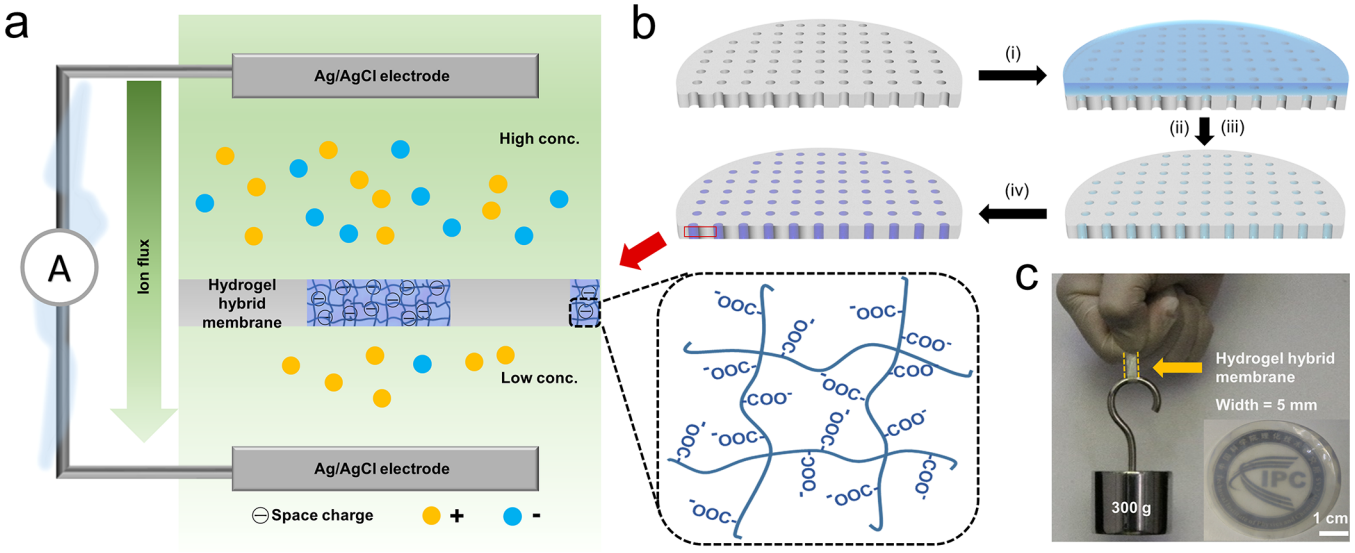

Figure 1. Illustration of the hydrogel hybrid membrane-based osmotic power generator. (a) Schematic depiction of the excellent cation selectivity of the hydrogel hybrid membrane benefiting from space charge. An osmotic power generator as the figure depicts can convert the salinity gradient to electric power. (b) Fabrication processes of the hydrogel hybrid membrane. (i) Precursor solution was poured on a PC film. (ii) Precursor solution filled the space of channels. (iii) The redundant solution was removed. (iv) The hydrogel was fabricated by UV irradiation. (c) Excellent mechanical property of the hydrogel hybrid membrane. The inset figure shows the whole view of the hydrogel hybrid membrane; the scale bar is 1 cm.

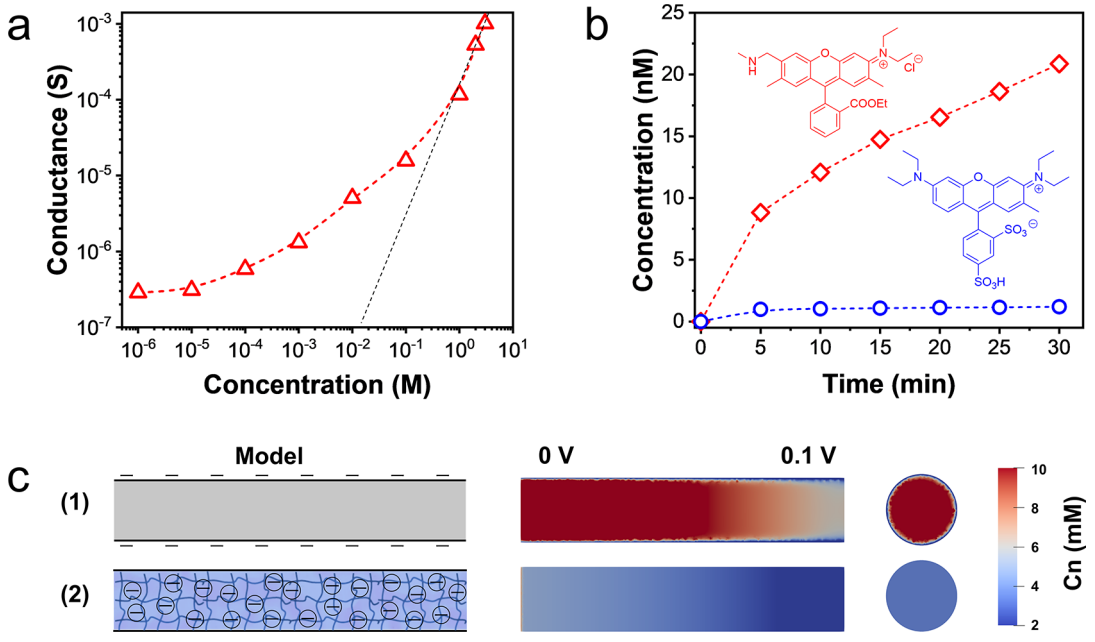

Figure 2. Ion transport properties of the hydrogel hybrid membrane. (a) Ion conductance of the 15% AAc/m membrane versus concentration, showing a charge-governed ion transport. (b) Permeability rate curves of rhodamine 6G (Rh (+), square symbols) and sulforhodamine (Rh (−), circular symbols), which indicate the excellent cation selectivity of the 15% AAc/m membrane. (c) Simulation results of anion concentration profiles of two models reveal the improved ion selectivity of the channel with space charge.

gradient, the hydrogel hybrid membrane-based osmotic power generator can convert osmotic energy to electric power efficiently; the power density reaches 11.72 W/m^2 by mimicking the salt-lake/river water conditions. Furthermore, the hydrogel hybrid membrane shows a prominent mechanical property, which is favorable for practical applications. This work investigates the ion transport in 1D hydrogel, meanwhile providing guidance for the design of high-performance membranes for sustainable power conversion, desalination, and water purification.

RESULTS AND DISCUSSION

The fabrication processes of the hydrogel hybrid membrane are shown in Figure 1b. To construct the hybrid membrane, precursor solution was poured on PC film (with cylindrical channels, pore density ~5 × 10^{12} m^{-2}), and precursor solution would penetrate the channels of PC via the capillary effect. After removing the redundant solution, precursors would only exist in channels and filled the space due to their hydrophilic characteristic. Lastly, AAc, AAm, and MMA would form the hydrogel network though free radical polymerization. This

https://dx.doi.org/10.1021/acscentsci.0c01054
ACS Cent. Sci. 2020, 6, 2097−2104

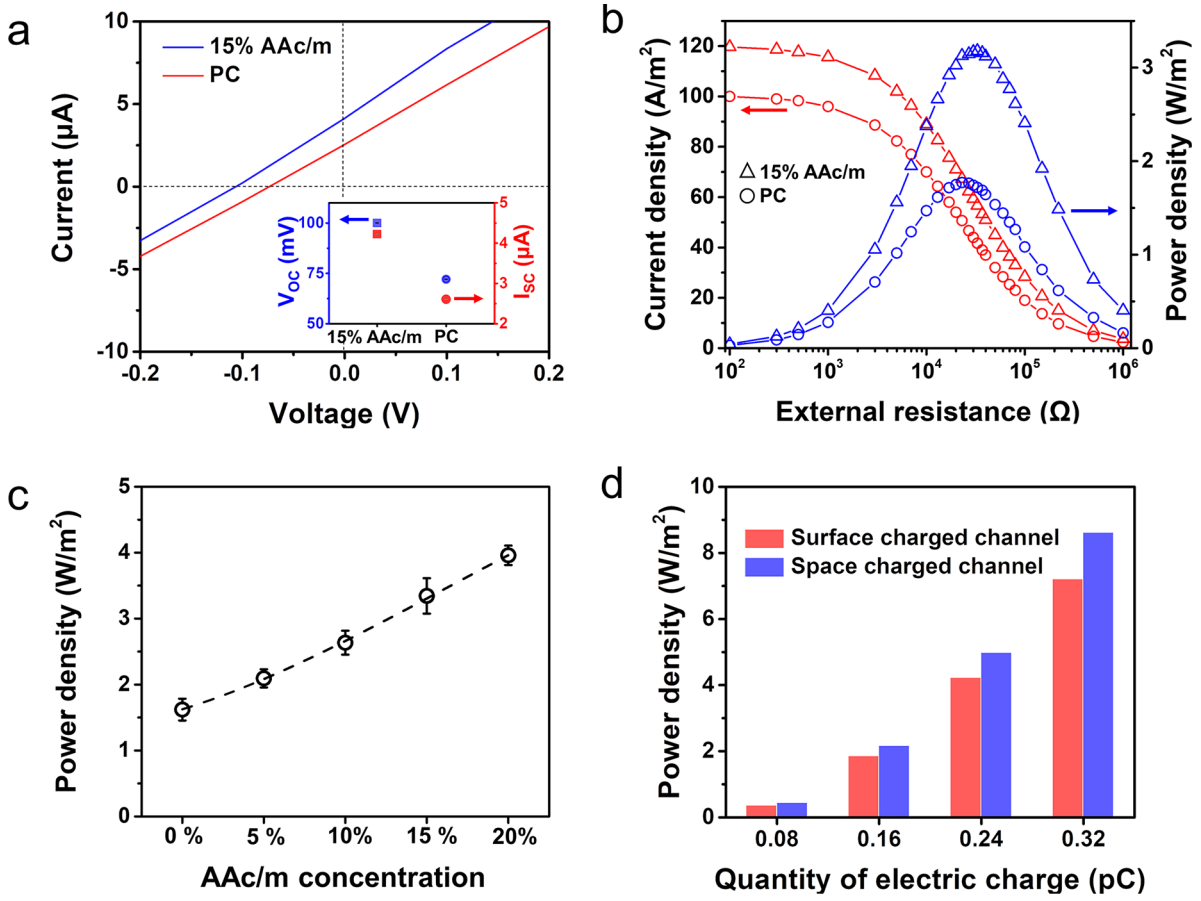

Figure 3. Significant improvement in osmotic energy conversion by using hydrogel hybrid membrane. (a) Open circuit voltage and short circuit current of the PC film and 15% AAc/m membrane at a 50-fold salinity gradient. The inset is their statistics. (b) Current densities and power densities of PC and the 15% AAc/m membrane at a 50-fold salinity gradient. (c) The statistical power density increases with AAc content. (d) Calculated output power of the surface charged nanochannel and space charged nanochannel.

kind of structure composed of hydrophilic-*co*-hydrophobic polymer chains could avoid the excessive swelling of the hydrogel,[24] which would be instrumental in keeping the construction and morphology of the hybrid membrane. The hydrogel hybrid membranes were denoted as *X*% AAc/m membrane (*X* refers to the mass fraction of AAc). As shown in Figure 1c, the hydrogel hybrid membrane with a width of 0.5 mm and thickness of 0.025 mm can lift up 300 g of weight, showing the outstanding mechanical property. As shown in Figures S1 and S2, the channels of the PC film are fully filled with hydrogel after hybridization. Additionally, the appearance of the C 1s peak at 288.8 eV (−COOH group) in the XPS spectrum (Figure S3),[25] the characteristic absorbance at 1700 and 1560 cm^{-1} (corresponding to −COOH and $-CONH_2$, respectively) in the FT-IR spectrum (Figure S4),[26] and confocal microscopy characterizations (Figure S5) all confirm the successful syntheses of the hydrogel hybrid membrane.

The characteristic of ion transport was measured by a current−voltage (*I*−*V*) measurement employing an electrochemical device (Figure S6). The hybrid membrane (15% AAc/m membrane) was nipped in two cells with different concentrations of potassium chloride (KCl) solution (from 10^{-6} to 3 M), and the electrodes were a pair of Ag/AgCl. Figure 2a shows the change of the membrane's ion conductance with the decrease of electrolyte concentration (red curve). The ion conductance of the hydrogel hybrid membrane deviates from the bulk behavior (black curve) obviously when the concentration is below 1 M, showing a charge-governed ion transport.[27] In a relatively low concentration, the curve is gentler for the increase of Debye length.[28] The ion selective property of the 15% AAc/m membrane was assessed with the help of the permeation of fluorescent dye (Figure 2b). The inset in Figure 2b shows the molecular formulas of fluorescent dyes (sulforhodamine and rhodamine 6G), which were selected for their similar structure but opposite charges. As a result, the concentration of rhodamine 6G (Rh (+)) increases distinctly with the test time, while the concentration of sulforhodamine (Rh (−)) remains quite low after 30 min. The transmembrane transport speed of Rh (+) is much larger than that of Rh (−), which indicates the excellent cation selectivity of the membrane. This high cation selectivity of the membrane can be illustrated by the space charge provided by the carboxylic group of the hydrogel 3D network.

To investigate the function of the space charge of 1D hydrogel, the theoretical simulation based on steady-state Poisson−Nernst−Plank (PNP) equations was performed (Note S1 and Figure S7).[29−31] Cylinder models (3D) with surface charge (1) or space charge (2) were designed. The calculation was carried out at a +0.1 V bias, and the profiles of surface charge and space charge were homogeneous. The anion concentration profiles of two channels are shown in Figure 2c. The longitudinal section of the surface charged channel shows a high anion concentration, which indicates its poor ion selectivity. However, the anion concentration in the space

https://dx.doi.org/10.1021/acscentsci.0c01054
ACS Cent. Sci. 2020, 6, 2097−2104

charged channel is low, showing the improved ion selectivity. As shown in the transversal section of the channels (Figure S8), the functional region of the ion-selective surface charged channel is only on its inner surface. The thickness of the Debye length (λ_D) can be calculated by eq 1:

$$\lambda_D = \sqrt{\frac{\varepsilon\varepsilon_0 RT}{2n_{bulk}Z^2F^2}} \quad (1)$$

where ε, ε_0, F, T, R, n_{bulk}, and Z are the permittivity of water, the permittivity of a vacuum, Faraday's constant, the absolute temperature, the universal gas constant, the concentration of solution, and the valence number, respectively.[28] λ_D in 0.01 M KCl solution is about 3.1 nm, whose scale is not compatible with PC channels. However, for the space charged channel, the charge not only is on the surface but also distributes in the whole channel region, and the influence of charge would be more effective. Therefore, the whole area of it could contribute to excellent cation selectivity (Figure S8).

Hydrogel hybrid membrane with outstanding cation selectivity can be used for harvesting the osmotic power from the gradient between seawater and river water. As shown in Figure 1a, two cells were filled with artificial seawater (0.5 M NaCl) and artificial river water (0.1 M NaCl), respectively, separated by the AAc/m membrane. In virtue of the cation selectivity, Na^+ would diffuse predominantly from the high-concentration cell (H-side) to the low-concentration cell (L-side), but Cl^- would be screened. The charges of the two sides would be different due to the asymmetric ion diffusion, leading to a continuous diffusion potential (E_{diff}). Then, the Gibbs free energy of the salinity gradient can be converted to electric energy by the reaction of electrodes connecting the external circuit.[32] First, $I-V$ measurements were performed to evaluate the open circuit voltage (V_{oc}) and short circuit current (I_{sc}) of the PC film (without modification) and 15% AAc/m membrane. Figure 3a shows the $I-V$ curves of the PC film and 15% AAc/m membrane, and the inset is the statistical data of V_{oc} and I_{sc}. The V_{oc} of the PC film is 72 mV, and the I_{sc} is 2.6 μA. This is due to the channel of the PC film being negative charged (−OH group) after the ion track-etched (Figure S9). After being filled with 1D hydrogel, the V_{oc} generated from the 15% AAc/m membrane is up to 100 mV, and the I_{sc} increases to 4.22 μA, which shows a clear improvement. The measured V_{oc} is the superposition effect of E_{diff} and redox potential (E_{redox}).[33] The contribution of E_{redox} during the process is discussed in Note S2, Figure S10, and Table S1. The energy conversion properties of membranes were further evaluated via an external circuit with an electrical load resistor (R_{el}).[34] The generated currents (I) were recorded, and the output power (P) can be calculated according to eq 2: $P = I^2 \times R_{el}$.[34] When the R_{el} is moderate (R_{el} = membrane resistance, R_m), the maximum output power can be obtained. As Figure 3b shows, the membrane resistance increases 30% after being filled with 1D hydrogel (thickness of 25 μm), which is low compared with the reported studies. For the energy conversion, the maximum output power density of the PC film is only 1.77 W/m^2, while that of 15% AAc/m is up to 3.18 W/m^2 (test area was approximately 3×10^4 μm^2, Figure S11). Benefiting from the preeminent cation selectivity attributed to the space charge of 1D hydrogel, the energy conversion of the hydrogel hybrid membrane improves substantially (~180%). Also, the corresponding energy conversion efficiencies were computed (Note S3 and Figure S12).

The relationship between electric quantity of the hydrogel and osmotic energy conversion was further analyzed. The total monomer content of hydrogel was kept at 20% for it would have a marked impact on the hydrogel network and ion transport.[35] As shown in Figure S13, the current density increases with the concentration of AAc. This result agrees with the statement that the high electric quantity contributes to a better ion selectivity and ion conductance. The maximum output densities of 0% AAc/m, 5% AAc/m, 10% AAc/m, 15% AAc/m, and 20% AAc/m are 1.54, 2.22, 2.78, 3.18, and 4.08 W/m^2, respectively (Figure 3c), which indicates that the output power density can be modulated by tuning the ratio of electriferous monomer. The energy conversion properties of hybrid membranes with different monomer contents were also discussed (Figure S14), which show that both the electric quantity and structure of the hydrogel network would influence the energy conversion.

In addition to the salinity gradient that arose by seawater and river water, wastewater extracted from oil drilling or brines generated by desalination plants can be used to harvest energy.[16] Therefore, the energy conversions in different salinity concentration gradients were measured. The salinity concentration (NaCl) in the L-side was kept at 10 mM, while the concentration in the H-side was changed from 20 mM to a saturated solution. The output power densities are shown in Figures S15 and S16. With the increase of salinity gradients, the output power density increases, and a maximum power density of 11.72 W/m^2 is achieved at a 500-fold salinity gradient. This demonstrates that the hydrogel hybrid membrane could still work at a high-concentration solution. Moreover, the stability was assessed by measuring the output power of the hybrid membrane immersed in water for 1−3 weeks (Figure S17), as well as a long-term run (Figure S18). As a result, the membrane retained an excellent power output indicating its outstanding stability. These experiments demonstrate that the combination of nanofluidics and hydrogel has great potential in enhancing the performance of osmotic power conversion.

To provide further physical insight into the effect of integrating hydrogels with nanochannels, steady-state Poisson−Nernst−Planck equations were performed (based on the 3D model, Note S1 and Figure S7).[29−31] In the simulation, the quantity of electric charge (Q) of the surface charged model and space charged model was set to the same value, and the value was selected according to the space charge density (σ_{spa}). σ_{spa} can be estimated by eq 3, $\sigma_{sur} = \frac{\varepsilon\varepsilon_0\xi}{\lambda_D}$ (σ_{sur} is the surface charge density), and eq 4, $\sigma_{spa} = \frac{\sigma_{sur}S}{V}$, where ξ, S, and V represent the ζ potential, superficial area, and volume.[36,37] The calculated σ_{spa} is about −4.46 C/cm^3, which is consistent with the reported data.[38] The quantity of electric charge can be obtained by eq 5, $Q = \sigma_{spa}V$,[39] which is approximately 0.18 pC. Therefore, Q was set from 0.08 to 0.32 pC (negative charge). The calculated output power densities of channels with surface charge and space charge are shown in Figure 3d and Table S2. As the value increases, the output power densities of the two models increase. Furthermore, the generated power of the space charged nanochannel is always higher than that of the surface charged. This indicates that constructing space charges is an effective and convenient method to improve the energy conversion efficiency.

https://dx.doi.org/10.1021/acscentsci.0c01054
ACS Cent. Sci. 2020, 6, 2097−2104

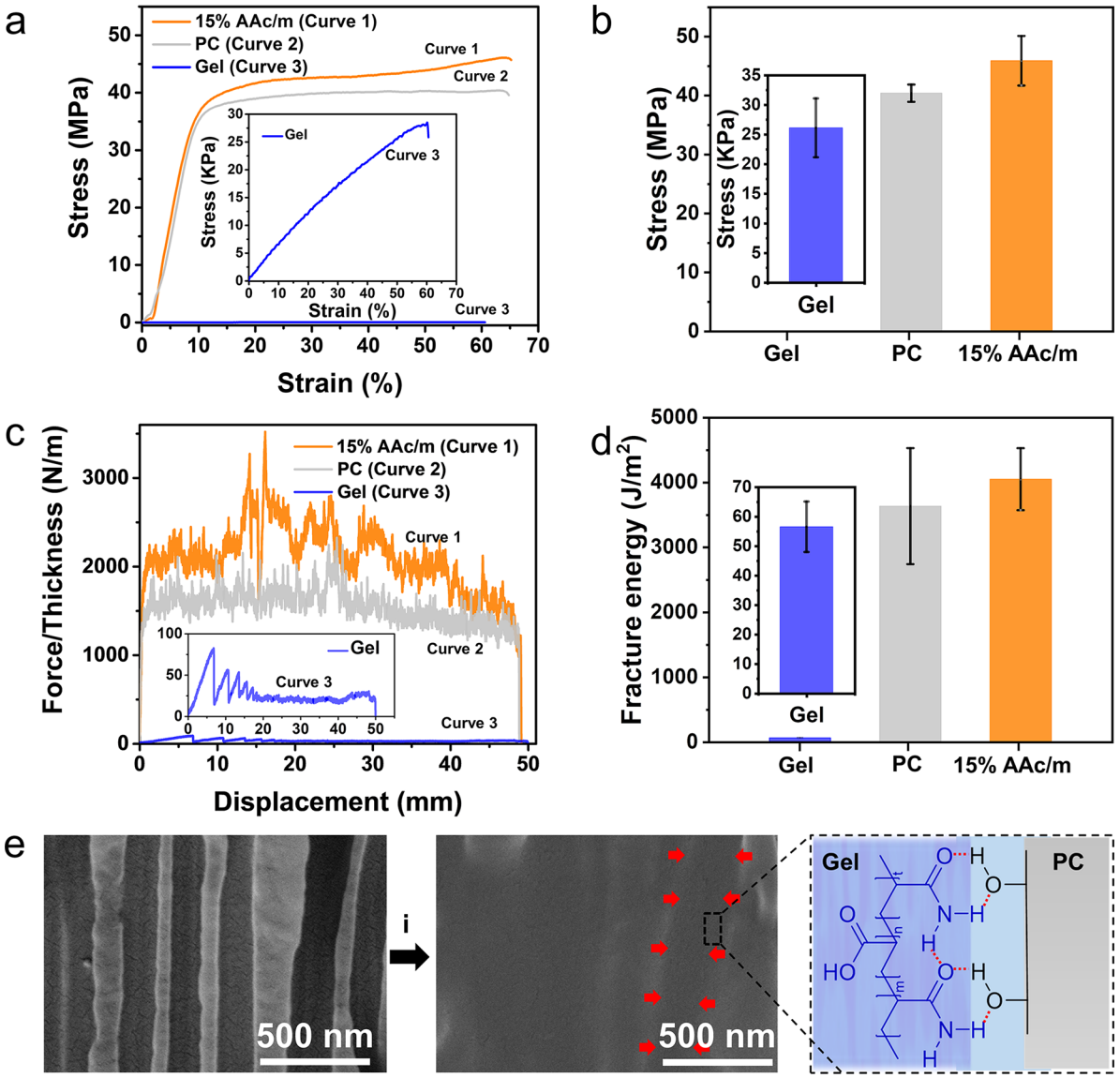

Figure 4. Mechanical properties of the hydrogel hybrid membrane. (a) Tensile stress of the hydrogel hybrid membrane (15% AAc/m), PC film, and pure hydrogel. (b) Statistical tensile stress of the membranes. (c) Tearing force curves of 15% AAc/m, PC film, and pure hydrogel. (d) Calculated toughness of the membranes. (e) Cross-section SEM images of the 15% AAc/m membrane before and after hybridization (i); the scale bar is 500 nm. The strong interface is formed by the hydrogen bonds between the hydrogel and channel.

The adequate mechanical strength of the membrane is an important factor for its practical application.[18] Therefore, the mechanical properties of the hydrogel hybrid membrane were evaluated. First, the mechanical properties of the 15% AAc/m membrane, PC film, and 15% AAc/m hydrogel were measured by the tensile test (Figure S19). The thickness of the hydrogel was 1 mm, while the thicknesses of the PC and hybrid membrane were 25 μm (Figure S20). As shown in Figure 4a, the strength of pure hydrogel is much lower than those of the PC and hybrid membrane. The strength changes from the kilopascal (kPa) level to megapascal (MPa) level after hybridization. Figure 4b shows the exact tensile stresses of the pure hydrogel, PC, and 15% AAc/m membrane, which are 26.10 kPa, 40.36 MPa, and 45.87 MPa, respectively. Then, the tearing test was performed to evaluate the toughness of membranes (Figure S21). The tear resistance of 15% AAc/m is much better than that of the hydrogel (Figure 4c). The fracture energy G can be calculated by eq 6: $G = 2F/s$, where s is the sample's thickness, and F is the average tearing force.[40] As Figure 4d shows, the fracture energy of hydrogel is only 57 J/m^2, while the fracture energy of 15% AAc/m is up to 4048 J/m^2 which increases 71-fold. It should be pointed out that both the tensile stress and fracture energy of 15% AAc/m are larger than those of PC, which indicates that the materials are not simply superposed. To illustrate the enhancement of mechanical properties, the cross-section of the 15% AAc/m membrane was observed. Figure 4e shows the channels' morphologies before and after the modification, and a strong interface between hydrogel and the channel wall is found. This is due to the fact that hydrogen bonds would form between amide groups of the hydrogel's network and hydroxyl groups of the channel wall.[41]

Durability is another important mechanical property of the membrane, and a friction test was carried out (Figure 5a). Figure 5b shows the wear curve of the 15% AAc/m membrane; the friction force maintains a low range after 100 cycles,

https://dx.doi.org/10.1021/acscentsci.0c01054
ACS Cent. Sci. 2020, 6, 2097−2104

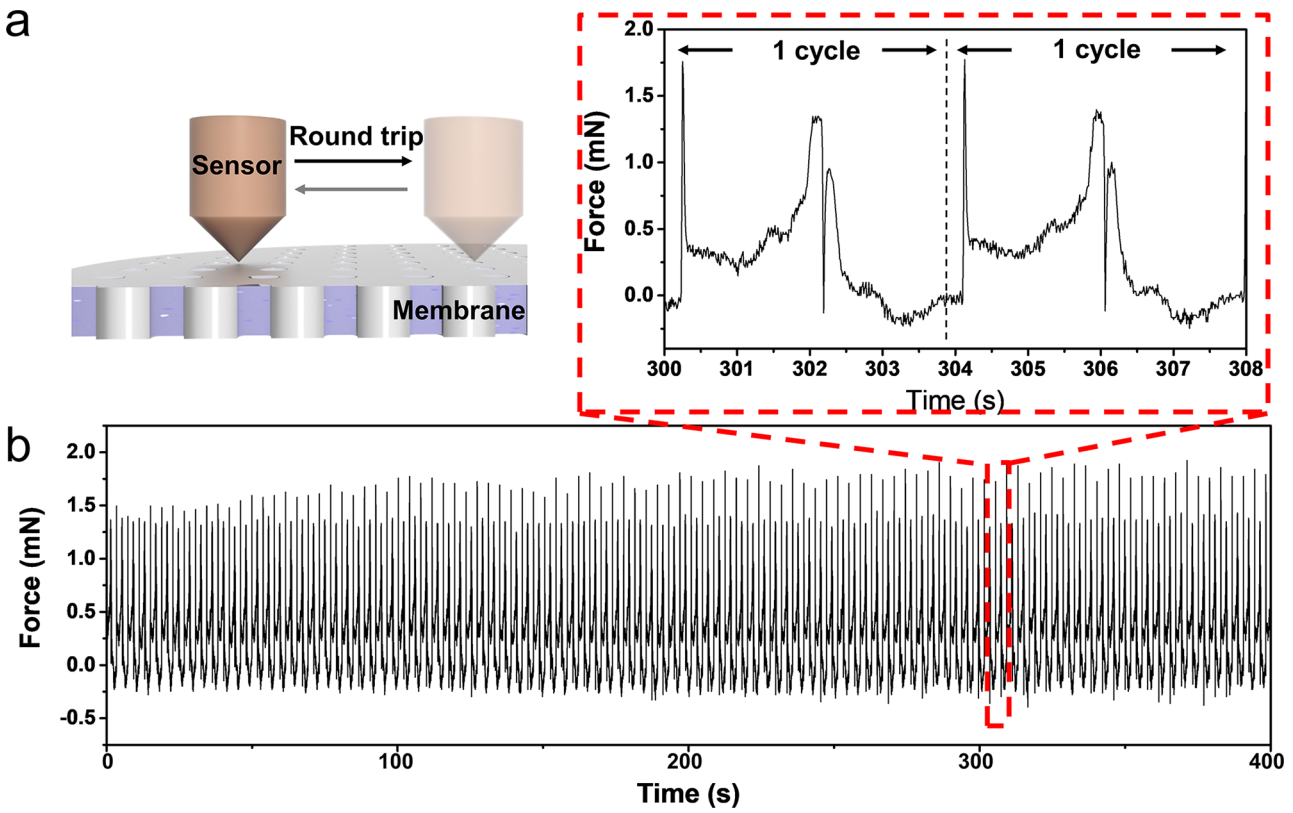

Figure 5. Durability of the hydrogel hybrid membrane. (a) The scheme illustrates the friction test. (b) Wear curve of the hydrogel hybrid membrane (15% AAc/m membrane). The friction force maintains a low range after 100 cycles.

showing the excellent durability. Another test using a rheometer was performed (Figure S22), and the membrane can still exhibit an outstanding performance after a probe friction for 100 cycles. This indicates that the PC film would not only provide channels for constructing the 1D hydrogel but also protect the hydrogel from being wrecked. Furthermore, the superoleophobic property underwater (Figure S23) and low oil adhesion force of the hydrogel hybrid membrane (Figure S24) would be propitious to resist the attachment of fouling organisms,[42,43] which is favorable for its long service.

CONCLUSION

In summary, we have revealed the ion transport and reverse electrodialysis of 1D hydrogel both experimentally and theoretically. Benefiting from the space negative charges of hydrogel and its unique network structure for ion transport, the hydrogel hybrid membrane exhibits an excellent cation selectivity, and the hydrogel hybrid membrane-based osmotic power generator outperforms the ordinary one in osmotic energy conversion. The power density is up to 4.08 W/m^2 by mixing artificial seawater and river water, and the maximum power density at a 500-fold salinity gradient is 11.72 W/m^2. The hydrogel hybrid membrane also exhibits excellent mechanical properties that are instrumental in maintaining the high performance. Moreover, the superoleophobic property and low oil adhesion force of the hybrid membrane could prevent it from being invalid caused by biofouling. This work provides a guidance for designing high-performance membrane systems in osmotic power generation and other mass transfer processes include desalination and water purification.

ASSOCIATED CONTENT

Supporting Information

The Supporting Information is available free of charge at https://pubs.acs.org/doi/10.1021/acscentsci.0c01054.

Methods, materials' structure and composition analysis, schematic diagram of the device, theoretical modeling, energy conversion of hydrogel hybrid membranes with different monomer concentrations, ζ potential, details of E_{diff} and E_{redox}, and wetting properties (PDF)

AUTHOR INFORMATION

Corresponding Author

Liping Wen − *Key Laboratory of Bio-Inspired Materials and Interfacial Science, Technical Institute of Physics and Chemistry, Chinese Academy of Sciences, Beijing 100190, P. R. China; University of Chinese Academy of Sciences, Beijing 100049, P. R. China;* orcid.org/0000-0001-8546-8988; Email: wen@mail.ipc.ac.cn

Authors

Weipeng Chen − *Key Laboratory of Bio-Inspired Materials and Interfacial Science, Technical Institute of Physics and Chemistry, Chinese Academy of Sciences, Beijing 100190, P. R. China; University of Chinese Academy of Sciences, Beijing 100049, P. R. China*

Qianru Zhang − *State Key Laboratory of Scientific and Engineering Computing, National Center for Mathematics and Interdisciplinary Sciences, Academy of Mathematics and Systems Science, Chinese Academy of Sciences, Beijing 100190, P. R. China; University of Chinese Academy of Sciences, Beijing 100049, P. R. China*

https://dx.doi.org/10.1021/acscentsci.0c01054
ACS Cent. Sci. 2020, 6, 2097−2104

Yongchao Qian − *Key Laboratory of Bio-Inspired Materials and Interfacial Science, Technical Institute of Physics and Chemistry, Chinese Academy of Sciences, Beijing 100190, P. R. China; Key Laboratory of Space Applied Physics and Chemistry Ministry of Education, Shanxi Key Laboratory of Macromolecular Science and Technology, School of Science, Northwestern Polytechnical University, Xi'an 710072, P. R. China*

Weiwen Xin − *Key Laboratory of Bio-Inspired Materials and Interfacial Science, Technical Institute of Physics and Chemistry, Chinese Academy of Sciences, Beijing 100190, P. R. China; University of Chinese Academy of Sciences, Beijing 100049, P. R. China*

Dezhao Hao − *Key Laboratory of Bio-Inspired Materials and Interfacial Science, Technical Institute of Physics and Chemistry, Chinese Academy of Sciences, Beijing 100190, P. R. China; University of Chinese Academy of Sciences, Beijing 100049, P. R. China*

Xiaolu Zhao − *Key Laboratory of Bio-Inspired Materials and Interfacial Science, Technical Institute of Physics and Chemistry, Chinese Academy of Sciences, Beijing 100190, P. R. China; University of Chinese Academy of Sciences, Beijing 100049, P. R. China*

Congcong Zhu − *Key Laboratory of Bio-Inspired Materials and Interfacial Science, Technical Institute of Physics and Chemistry, Chinese Academy of Sciences, Beijing 100190, P. R. China; University of Chinese Academy of Sciences, Beijing 100049, P. R. China*

Xiang-Yu Kong − *Key Laboratory of Bio-Inspired Materials and Interfacial Science, Technical Institute of Physics and Chemistry, Chinese Academy of Sciences, Beijing 100190, P. R. China;* orcid.org/0000-0002-4475-2162

Benzhuo Lu − *State Key Laboratory of Scientific and Engineering Computing, National Center for Mathematics and Interdisciplinary Sciences, Academy of Mathematics and Systems Science, Chinese Academy of Sciences, Beijing 100190, P. R. China; University of Chinese Academy of Sciences, Beijing 100049, P. R. China;* orcid.org/0000-0003-4159-1532

Lei Jiang − *Key Laboratory of Bio-Inspired Materials and Interfacial Science, Technical Institute of Physics and Chemistry, Chinese Academy of Sciences, Beijing 100190, P. R. China; University of Chinese Academy of Sciences, Beijing 100049, P. R. China*

Complete contact information is available at: https://pubs.acs.org/10.1021/acscentsci.0c01054

Author Contributions

L.W. proposed the research direction and guided the project. W.C. designed and performed the experiments. X.-Y.K., L.W., X.-Y.K. and W.C. analyzed and discussed the experimental results and drafted the manuscript. Y.Q., W.X., D.H., X.Z., C.Z., and L.J. joined the discussion of data and gave useful suggestions. Q.Z. and B.L. performed the theoretical simulations. All authors contributed to the writing of the manuscript.

Notes

The authors declare no competing financial interest.

■ ACKNOWLEDGMENTS

This work was supported by the National Key R&D Program of China (2017YFA0206904, 2017YFA0206900, 2016YFB0201304), the National Natural Science Foundation of China (21625303, 21905287, 51673206, 21988102, 21573274, 11771435), the Strategic Priority Research Program of the Chinese Academy of Sciences (XDA21010213), Beijing Natural Science Foundation (2194088), and the Key Research Program of the Chinese Academy of Sciences (QYZDY-SSW-SLH014).

■ REFERENCES

(1) Daiguji, H.; Yang, P.; Majumdar, A. Ion Transport in Nanofluidic Channels. *Nano Lett.* **2004**, *4* (1), 137−142.

(2) Xiao, K.; Giusto, P.; Wen, L.; Jiang, L.; Antonietti, M. Nanofluidic Ion Transport and Energy Conversion through Ultrathin Free-standing Polymeric Carbon Nitride Membranes. *Angew. Chem., Int. Ed.* **2018**, *57* (32), 10123−10126.

(3) Perez-Mitta, G.; Marmisolle, W. A.; Trautmann, C.; Toimil-Molares, M. E.; Azzaroni, O. Nanofluidic Diodes with Dynamic Rectification Properties Stemming from Reversible Electrochemical Conversions in Conducting Polymers. *J. Am. Chem. Soc.* **2015**, *137* (49), 15382−15385.

(4) Ali, M.; Nasir, S.; Ramirez, P.; Ahmed, I.; Nguyen, Q. H.; Fruk, L.; Mafe, S.; Ensinger, W. Optical Gating of Photosensitive Synthetic Ion Channels. *Adv. Funct. Mater.* **2012**, *22* (2), 390−396.

(5) He, X.; Zhang, K.; Liu, Y.; Wu, F.; Yu, P.; Mao, L. Chaotropic Monovalent Anion-Induced Rectification Inversion at Nanopipettes Modified by Polyimidazolium Brushes. *Angew. Chem., Int. Ed.* **2018**, *57* (17), 4590−4593.

(6) Xiao, K.; Xie, G.; Zhang, Z.; Kong, X.; Liu, Q.; Li, P.; Wen, L.; Jiang, L. Enhanced Stability and Controllability of an Ionic Diode Based on Funnel-Shaped Nanochannels with an Extended Critical Region. *Adv. Mater.* **2016**, *28* (17), 3345−3350.

(7) Acar, E. T.; Buchsbaum, S. F.; Combs, C.; Fornasiero, F.; Siwy, Z. S. Biomimetic Potassium-selective Nanopores. *Sci. Adv.* **2019**, *5* (2), No. eaav2568.

(8) Zhang, Z.; Wen, L.; Jiang, L. Bioinspired Smart Asymmetric Nanochannel Membranes. *Chem. Soc. Rev.* **2018**, *47* (2), 322−356.

(9) Amy, G.; Ghaffour, N.; Li, Z.; Francis, L.; Linares, R. V.; Missimer, T.; Lattemann, S. Membrane-based Seawater Desalination: Present and Future Prospects. *Desalination* **2017**, *401*, 16−21.

(10) Zhang, M.; Guo, R.; Chen, K.; Wang, Y.; Niu, J.; Guo, Y.; Zhang, Y.; Yin, Z.; Xia, K.; Zhou, B.; Wang, H.; He, W.; Liu, J.; Sitti, M.; Zhang, Y. Microribbons Composed of Directionally Self-assembled Nanoflakes as Highly Stretchable Ionic Neural Electrodes. *Proc. Natl. Acad. Sci. U. S. A.* **2020**, *117* (26), 14667−14675.

(11) Zhang, Z.; Zhang, P.; Yang, S.; Zhang, T.; Loffler, M.; Shi, H.; Lohe, M. R.; Feng, X. Oxidation Promoted Osmotic Energy Conversion in Black Phosphorus Membranes. *Proc. Natl. Acad. Sci. U. S. A.* **2020**, *117* (25), 13959−13966.

(12) Xin, W.; Zhang, Z.; Huang, X.; Hu, Y.; Zhou, T.; Zhu, C.; Kong, X. Y.; Jiang, L.; Wen, L. High-performance Silk-based Hybrid Membranes Employed for Osmotic Energy Conversion. *Nat. Commun.* **2019**, *10* (1), 3876.

(13) Chen, J.; Xin, W.; Kong, X.-Y.; Qian, Y.; Zhao, X.; Chen, W.; Sun, Y.; Wu, Y.; Jiang, L.; Wen, L. Ultrathin and Robust Silk Fibroin Membrane for High-Performance Osmotic Energy Conversion. *ACS Energy Lett.* **2020**, *5* (3), 742−748.

(14) Li, R.; Jiang, J.; Liu, Q.; Xie, Z.; Zhai, J. Hybrid Nanochannel Membrane Based on Polymer/MOF for Highperformance Salinity Gradient Power Generation. *Nano Energy* **2018**, *53*, 643−649.

(15) Chen, C.; Liu, D.; He, L.; Qin, S.; Wang, J.; Razal, J. M.; Kotov, N. A.; Lei, W. Bio-inspired Nanocomposite Membranes for Osmotic Energy Harvesting. *Joule* **2020**, *4* (1), 247−261.

(16) Macha, M.; Marion, S.; Nandigana, V. V. R.; Radenovic, A. 2D Materials as an Emerging Platform for Nanopore-based Power Generation. *Nat. Rev. Mater.* **2019**, *4* (9), 588−605.

(17) Graf, M.; Lihter, M.; Unuchek, D.; Sarathy, A.; Leburton, J. P.; Kis, A.; Radenovic, A. Light-Enhanced Blue Energy Generation Using MoS_2 Nanopores. *Joule* **2019**, *3* (6), 1549−1564.

(18) Zhu, X.; Hao, J.; Bao, B.; Zhou, Y.; Zhang, H.; Pang, J.; Jiang, Z.; Jiang, L. Unique Ion Rectification in Hypersaline Environment: A

High-performance and Sustainable Power Generator System. *Sci. Adv.* **2018**, *4* (10), No. eaau1665.
(19) Bao, B.; Hao, J.; Bian, X.; Zhu, X.; Xiao, K.; Liao, J.; Zhou, J.; Zhou, Y.; Jiang, L. 3D Porous Hydrogel/Conducting Polymer Heterogeneous Membranes with Electro-/pH-Modulated Ionic Rectification. *Adv. Mater.* **2017**, *29* (44), 1702926.
(20) Chen, W.; Wang, Q.; Chen, J.; Zhang, Q.; Zhao, X.; Qian, Y.; Zhu, C.; Yang, L.; Zhao, Y.; Kong, X.-Y.; Lu, B.; Jiang, L.; Wen, L. Improved Ion Transport and High Energy Conversion through Hydrogel Membrane with 3D Interconnected Nanopores. *Nano Lett.* **2020**, *20*, 5705.
(21) Schroeder, T. B. H.; Guha, A.; Lamoureux, A.; VanRenterghem, G.; Sept, D.; Shtein, M.; Yang, J.; Mayer, M. An Electric-eel-inspired Soft Power Source from Stacked Hydrogels. *Nature* **2017**, *552* (7684), 214−218.
(22) Catania, K. C. Electric Eels Concentrate Their Electric Field to Induce Involuntary Fatigue in Struggling Prey. *Curr. Biol.* **2015**, *25* (22), 2889−2898.
(23) Zhao, Z.; Fang, R.; Rong, Q.; Liu, M. Bioinspired Nanocomposite Hydrogels with Highly Ordered Structures. *Adv. Mater.* **2017**, *29* (45), 1703045.
(24) Kondo, S.; Hiroi, T.; Han, Y.-S.; Kim, T.-H.; Shibayama, M.; Chung, U.-I.; Sakai, T. Reliable Hydrogel with Mechanical "Fuse Link" in an Aqueous Environment. *Adv. Mater.* **2015**, *27* (45), 7407−7411.
(25) Su, X.; Hao, D.; Li, Z.; Guo, X.; Jiang, L. Design of Hierarchical Comb Hydrophilic Polymer Brush (HCHPB) Surfaces Inspired by Fish Mucus for Anti-biofouling. *J. Mater. Chem. B* **2019**, *7* (8), 1322−1332.
(26) Wang, J.; Zhang, W.; Qian, Y.; Deng, B.; Tian, W. pH, Temperature, and Magnetic Triple-responsive Polymer Porous Microspheres for Tunable Adsorption. *Macromol. Mater. Eng.* **2016**, *301* (9), 1132−1141.
(27) Zhang, Z.; Xie, G.; Xiao, K.; Kong, X.-Y.; Li, P.; Tian, Y.; Wen, L.; Jiang, L. Asymmetric Multifunctional Heterogeneous Membranes for pH- and Temperature-Cooperative Smart Ion Transport Modulation. *Adv. Mater.* **2016**, *28* (43), 9613−9619.
(28) Schoch, R. B.; Han, J.; Renaud, P. Transport Phenomena in Nanofluidics. *Rev. Mod. Phys.* **2008**, *80* (3), 839−883.
(29) Tu, B.; Chen, M.; Xie, Y.; Zhang, L.; Eisenberg, B.; Lu, B. A Parallel Finite Element Simulator for Ion Transport through Three-dimensional Ion Channel Systems. *J. Comput. Chem.* **2013**, *34* (24), 2065−2078.
(30) Tu, B.; Xie, Y.; Zhang, L.; Lu, B. Stabilized Finite Element Methods to Simulate the Conductances of Ion Channels. *Comput. Phys. Commun.* **2015**, *188*, 131−139.
(31) Liu, X.; Lu, B. Incorporating Born Solvation Energy into the Three-dimensional Poisson-Nernst-Planck Model to Study Ion Selectivity in KcsA K^+ Channels. *Phys. Rev. E: Stat. Phys., Plasmas, Fluids, Relat. Interdiscip. Top.* **2017**, *96* (6), 062416.
(32) Tedesco, M.; Hamelers, H. V. M.; Biesheuvel, P. M. Nernst-Planck Transport Theory for (Reverse) Electrodialysis: I. Effect of Co-ion Transport through the Membranes. *J. Membr. Sci.* **2016**, *510*, 370−381.
(33) Ouyang, W.; Wang, W.; Zhang, H.; Wu, W.; Li, Z. Nanofluidic Crystal: a Facile, High-efficiency and High-power-density Scaling up Scheme for Energy Harvesting Based on Nanofluidic Reverse Electrodialysis. *Nanotechnology* **2013**, *24* (34), 345401.
(34) Zhang, Z.; Sui, X.; Li, P.; Xie, G.; Kong, X.-Y.; Xiao, K.; Gao, L.; Wen, L.; Jiang, L. Ultrathin and Ion-Selective Janus Membranes for High-performance Osmotic Energy Conversion. *J. Am. Chem. Soc.* **2017**, *139* (26), 8905−8914.
(35) Zhao, F.; Zhou, X.; Shi, Y.; Qian, X.; Alexander, M.; Zhao, X.; Mendez, S.; Yang, R.; Qu, L.; Yu, G. Highly Efficient Solar Vapour Generation via Hierarchically Nanostructured Gels. *Nat. Nanotechnol.* **2018**, *13* (6), 489−495.
(36) Wang, X.; Tsuru, T.; Nakao, S.; Kimura, S. Electrolyte Transport through Nanofiltration Membranes by the Space-charge Model and the Comparison with Teorell-Meyer-Sievers Model. *J. Membr. Sci.* **1995**, *103* (1), 117−133.
(37) Schaep, J.; Vandecasteele, C. Evaluating the Charge of Nanofiltration Membranes. *J. Membr. Sci.* **2001**, *188* (1), 129−136.
(38) Zhang, Z.; Yang, S.; Zhang, P.; Zhang, J.; Chen, G.; Feng, X. Mechanically Strong MXene/Kevlar Nanofiber Composite Membranes as High-performance Nanofluidic Osmotic Power Generators. *Nat. Commun.* **2019**, *10* (1), 2920.
(39) Serway, R. A.; Jewett, J. W. Electric Field of a Continuous Charge Distribution. In *Physics for Scientists and Engineers*, 9th ed.; Dodd, E., Ed.; Cengage Learning: Boston, 2014; pp 704−708.
(40) Huang, Y.; King, D. R.; Sun, T.; Nonoyama, T.; Kurokawa, T.; Nakajima, T.; Gong, J. Energy-dissipative Matrices Enable Synergistic Toughening in Fiber Reinforced Soft Composites. *Adv. Funct. Mater.* **2017**, *27* (9), 1605350.
(41) Ye, Y.; Frauenlob, M.; Wang, L.; Tsuda, M.; Sun, T.; Cui, K.; Takahashi, R.; Zhang, H.; Nakajima, T.; Nonoyama, T.; Kurokawa, T.; Tanaka, S.; Gong, J. Tough and Self-recoverable Thin Hydrogel Membranes for Biological Applications. *Adv. Funct. Mater.* **2018**, *28* (31), 1801489.
(42) Tesler, A.; Kim, P.; Kolle, S.; Howell, C.; Ahanotu, O.; Aizenberg, J. Extremely Durable Biofouling-resistant Metallic Surfaces Based on Electrodeposited Nanoporous Tungstite Films on Steel. *Nat. Commun.* **2015**, *6*, 8649.
(43) Chen, W.; Hao, D.; Guo, X.; Hao, W.; Jiang, L. Preventing Diatom Adhesion Using a Hydrogel with an Orthosilicic Acid Analog as a Deceptive Food. *J. Mater. Chem. A* **2018**, *6* (39), 19125−19132.

https://dx.doi.org/10.1021/acscentsci.0c01054
ACS Cent. Sci. 2020, 6, 2097−2104